JOURNAL OF MATERIALS SCIENCE 32 (1997) 609–617

Effect of hydrogen on the tensile ductility of Ti6Al4V

Part II *Fracture of pre-cracked tensile specimens*

J. GU*, D. HARDIE
Department of Mechanical, Materials and Manufacturing Engineering, The University, Newcastle-upon-Tyne NE1 7RU, UK

Pre-cracked compact tensile specimens of Ti6Al4V charged with hydrogen were slowly strained in tension at room temperature and 2.3×10^{-5} mm s^{-1} and a crack-growth monitor used to detect the early stages of slow crack growth and so confirm the load for its initiation. The micro-fractography and crack propagation path were examined by scanning electron microscopy (SEM). The results confirmed that slow cracking preceded fast cracking in all specimens and at hydrogen contents below 90 p.p.m. the stress intensity factor for slow cracking, K_s, increased with increasing hydrogen, whereas it was reduced at higher levels. The average slow crack growth rate increased on increasing the hydrogen content from 10 p.p.m. to 90 p.p.m., but decreased sharply as the hydrogen content was further increased to 125 p.p.m., and then again increased above 125 p.p.m. hydrogen, but only very slowly. With increasing hydrogen content, the slow crack initiation changed from within the α phase to the interface between the α and β phases, the growth path from transgranular to interfacial separation and the fracture mode from the mixed ductile and cleavage to fracture along the α–β interface ($\geqslant$ 500 p.p.m.). It is suggested that the mechanism of slow crack growth is different for the different ranges of hydrogen content: at the low hydrogen levels ($<$ 90 p.p.m.) the dominant mechanism is creep-induced slow crack growth, whereas the slow cracking becomes controlled by hydrogen diffusion in both α and β phases when the hydrogen content is above 90 p.p.m. Fast fracture was invariably preceded by slow crack growth at all hydrogen levels up to 500 p.p.m.

1. Introduction

Ti6Al4V is by far the most important and widely used titanium alloy in many industries, including aerospace applications, marine engineering, energy production and storage, and biomedical applications [1]. From the point of view of reliable service, there is an increased requirement for the prediction of fracture properties in structural components, such as fracture toughness, K_{Ic}, the threshold stress intensity factor for slow crack growth and the effect of environment on crack growth rate. In addition, because any improvement in these properties can result in more efficient design with attendant weight savings, it is clearly worthwhile to identify those parameters that influence such fracture properties. These include preferred orientation, micro-structure and environment, especially hydrogen.

The effect of hydrogen on the fracture behaviour of titanium alloys has been most extensively studied [2–18]. These studies have involved the action of both internal [2–6, 14, 16, 17] and environmental hydrogen [7–13], the effect of hydrogen on the threshold stress intensity factor and fracture toughness [2–6], the dynamics of sub-critical cracking growth [10, 14–17], and hydrogen-induced fractography [11, 12, 18]. The work has generally involved constant displacement [10, 14] or sustained load techniques [2, 3, 5, 7]. Although the first is suitable for determination of the slow crack growth rate, the latter requires many specimens and a long time to obtain the threshold stress intensity factor. In addition, the range of hydrogen contents used by earlier investigators is either narrow [2, 3] or not systematic [4, 5], so that the conclusions drawn by different authors frequently show pronounced disagreement.

From the early 1960s, Parkins and his colleagues [19–22] have developed and utilized a slow strain-rate technique (SSRT) for the study of stress corrosion cracking (SCC). The chief advantage of this technique [19] is that it is much more positive in producing SCC than conventional constant displacement or constant load tests, so that the testing time is inevitably reduced. Not only can this method satisfy pass/fail criteria, but it can also provide data concerning the effect

* *Permanent address*: Department of Materials Science and Engineering, Tsinghua University, Beijing, People's Republic of China.

0022–2461

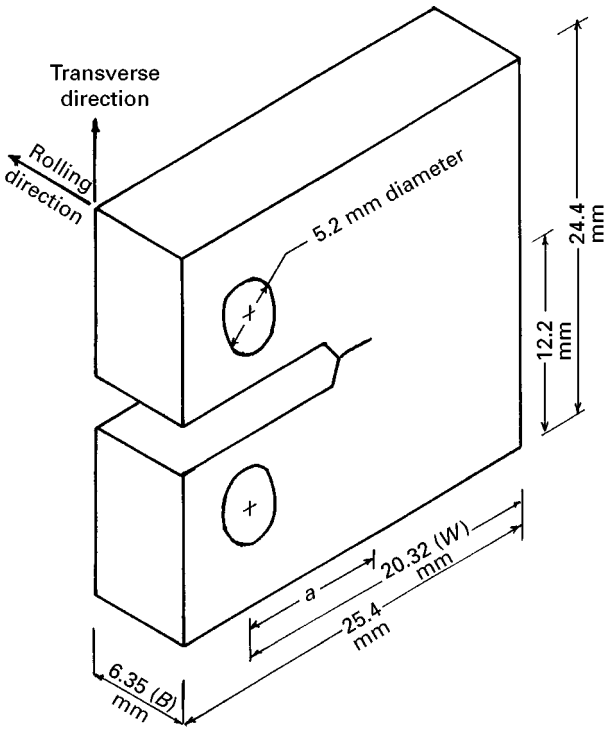

Figure 1 Design of compact tension specimen.

of various parameters on SCC susceptibility. The significantly better reproducibility of the cracking velocities determined from SSRT, as compared to those from constant load tests, is also noteworthy.

In the present work, SSRT of pre-cracked compact tensile specimens was employed to examine the effects of internal hydrogen on the fracture properties of mill-annealed Ti6Al4V round bar. This allowed a wider range of hydrogen content to be studied, from 10–500 p.p.m., with a satisfactory number of points between these limits. The fractography and crack propagation paths were observed by SEM.

2. Experimental procedure

The material received was hot-rolled 110 mm diameter round bar, containing 6.55 Al, 4.19 V, 0.19 Fe, 0.185 O, 0.007 N, 0.02 C, 0.001 H and balance Ti (wt %). The microstructure consisted of equiaxed primary α phase (grain size about 20 μm) with β phase, and a eutectoid structure of α and β phases discontinuously dispersed in the boundaries. The micrography revealed that some α grains were elongated in various directions, as has been previously shown [23].

Compact tensile (CT) specimens (Fig. 1) were cut from the bar with a specific orientation having the major plane perpendicular to the longitudinal direction of the round bar and the notches always parallel to a particular transverse (T) direction (as specified previously [23]), so that the fracture plane was parallel to the longitudinal axis of the original bar and propagation was in the specific transverse direction. Although the specimen thickness $B = 6.35$ mm does not fulfil the requirements of British Standard BS5447 [24] for plane strain fracture toughness measurements, nevertheless this type of specimen was considered acceptable for comparative purposes. Specimens finished to a 5/0 grit were then pre-cracked by fatigue in a relatively hard fatigue machine at a frequency of 150 Hz before charging with hydrogen. The maximum stress intensity factor used for the specimens in the final stage of fatigue pre-cracking was always less than 50% of the critical stress intensity factor for the final failure.

Specimens were carefully washed in acetone, dried and weighed before placing in the charging furnace which was then sealed and evacuated to $< 10^{-4}$ mbar, before heating to 600 °C. After a good vacuum had been achieved, the system was isolated from the pumps and purified hydrogen was collected in a gas burette so that appropriate measured amounts could be bled into the furnace containing the specimen. The furnace was then held at 600 °C for 2 h before cooling. The hydrogen content, C (p.p.m. by wt) in the specimen was calculated from the following formula

$$C = \frac{10^3 A_H P_1 V_1 T_0}{22.4\, G\, P_0\, T_1} \quad (1)$$

where A_H is the molecular weight of hydrogen, T_0 the standard temperature, 273 K, P_0 the standard pressure (1 bar), T_1 the ambient temperature (K), P_1 the environment pressure at ambient temperature, V_1 the hydrogen volume added (cm^3) and G the weight of the specimen (g).

The holding time of 2 h at 600 °C ensured homogeneity of distribution of hydrogen in the specimen and the microstructures of the specimens heated and charged at 600 °C for 2 h were essentially unchanged, except at the higher hydrogen levels.

The slow straining of compact tensile (CT) specimens was conducted in a vertically mounted tensile machine at a crosshead speed of 2.3×10^{-5} mm s^{-1}. The outputs from the load cell, P, and the displacement from a clip gauge, δ_g, were fed, respectively, into an X–Y (load–displacement) recorder and an X–t (load–time) recorder, which allowed subsequent plotting of load–displacement and load–time curves. A crack growth monitor CGM5 using a.c. impedance measurements was used to detect the early stages of slow crack growth in pre-cracked CT specimens, and a potential output from the CGM5 was fed into an X–t (potential output versus time) recorder and the potential–time curve plotted, to allow comparison with load and displacement measurements. The initiation of slow crack growth can thus be determined from the potential time curve and the initial load, P_s, for slow crack growth can be assessed from the load–time curve. The load, P_H, for fast cracking was directly obtained from the load–displacement curve.

The initial and final crack lengths for the period of slow crack growth were measured at ten positions along the crack fronts (fatigue and slow cracking) on the fracture surface and the averages of the measurements for each crack front used to obtain the effective initial crack length for slow cracking as (the distance from the loading line to the fatigue crack tip) and the effective crack length for fast fracture, a_s (the distance

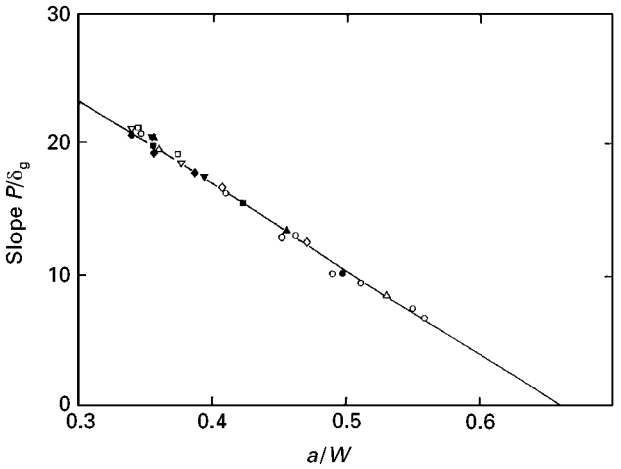

Figure 2 Calibration curve relating compliance to crack length. [H] (p.p.m.); (○) 10, (●) 30, (△) 53; (▲) 90; (▽) 125, (▼) 165, (□) 200, (◆) 250, (■) 358, (◇) 500.

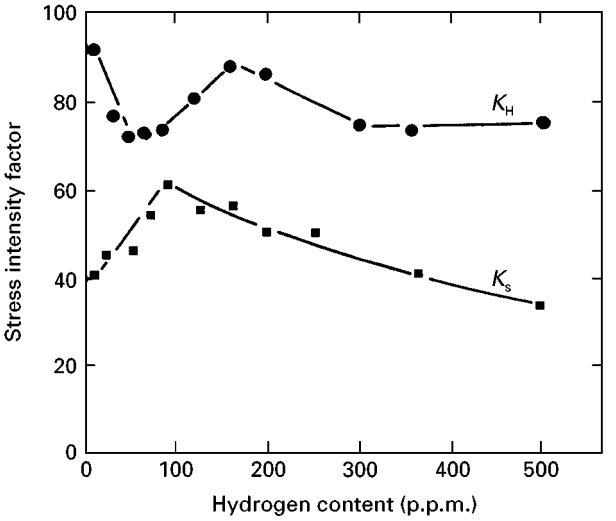

Figure 3 Effect of hydrogen on the threshold stress intensity factor for slow crack initiation, K_s, and the critical stress intensity factor for fast cracking, K_H.

from the loading line to the end of the slow crack growth).

The stress intensity factor, K, was calculated from the standard equation for this particular specimen geometry [24]

$$K = \frac{PY}{BW^{1/2}} \tag{2a}$$

where

$$Y = 29.6\left(\frac{a}{W}\right)^{1/2} - 185.5\left(\frac{a}{W}\right)^{3/2} + 655.7\left(\frac{a}{W}\right)^{5/2} - 1017\left(\frac{a}{W}\right)^{7/2} + 638.9\left(\frac{a}{W}\right)^{9/2} \tag{2b}$$

where P is the load, a the crack length, B the specimen thickness and W the net width of the specimen from the loading line (Fig. 1). K_s and K_H, the critical stress intensity factors for slow crack growth and unstable fast cracking, respectively, can then be determined.

It is common practice [25] to refer to the ratio δ/P as the compliance, where P is the applied load and δ is the displacement at the loading line for a brittle solid. The curve of compliance against crack growth, a (or a/W), is usually employed to obtain the relationship between the crack length and the stress intensity factor. For convenience, the relationship between the slope P/δ_g of the load–displacement curve and a/W was employed in this study to assess the crack length, using the actual opening, δ_g, at the knife edges under loading. A series of specimens having various crack lengths was used to obtain a calibration curve (Fig. 2) and the relationship $(P/\delta_g) = 42.52 - 64.55(a/W)$ derived from this (with a high correlation coefficient). When the data from specimens containing different hydrogen contents were compared with the line obtained it became obvious that the variation in hydrogen content did not have any effect, i.e. this plot may be considered unique for this material, whatever the hydrogen content. Using the experimental curves (P versus δ_g) together with the relationship between P/δ_g and a/W, and Equation 2, the stress intensity factor, K, at a certain crack length, a, may be determined. Thus the relationship between the $\Delta K_s (= K - K_s)$ and $\Delta a (= a_H - a_s)$ may be obtained.

The average velocity of the slow crack growth was also calculated by dividing the slow crack length Δa $(= a_H - a_s)$ by the slow cracking time $\Delta t (= t_H - t_s)$.

The slow crack growth path was examined using scanning electron microscopy (SEM) in the back-scatter electron image mode. The specimens used were ground to 600 grit before polishing to 1 μm diamond finish but not etched. Because the compositions of the α and β phases of Ti6Al4V are different [26], the microstructures are clearly revealed by the mass image.

3. Results

Slow cracking occurs in all specimens, whatever the hydrogen content (Fig. 3), but the effect of hydrogen content on K_s may be divided into two parts, below and above 90 p.p.m. In the low hydrogen range, K_s increases with increasing hydrogen content but, in contrast, K_s decreases as hydrogen increases at higher hydrogen levels. The mean velocity for slow cracking rises sharply with increasing hydrogen up to 90 p.p.m. then drops suddenly, by more than an order of magnitude, and only increases very gradually with hydrogen content up to 500 p.p.m. (Fig. 4). There seem to be three distinct ranges for fast fracture: K_H increases with hydrogen up to about 50 p.p.m. and remains constant to about 90 p.p.m., then increases to a maximum between 90 and 250 p.p.m. before dropping to the same constant value above 250 p.p.m.

The slopes of curves relating ΔK and Δa during slow crack growth for specimens having different hydrogen contents show a decrease from 10 p.p.m. to 90 p.p.m. but above 125 p.p.m. become reasonably constant at a value just greater than that for the as-received material (Fig. 5). The macro-characteristics of the fracture surfaces are obviously influenced by hydrogen content (Table I). The fractography of the

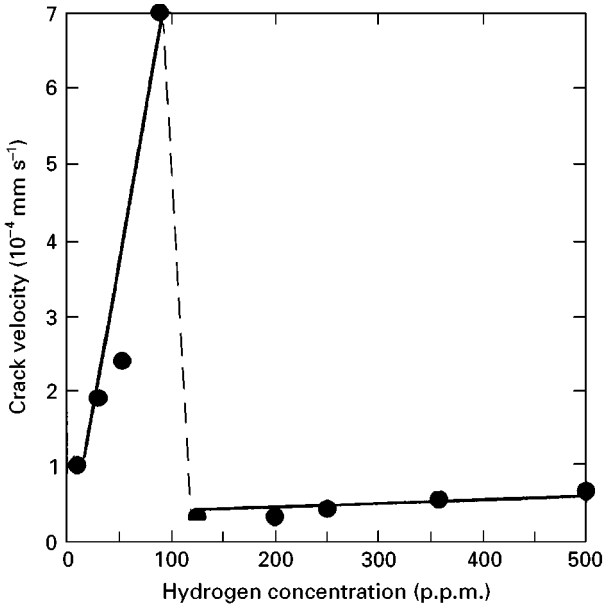

Figure 4 Effect of hydrogen on the mean velocity of slow cracking when straining at 2.3×10^{-5} mm s^{-1}.

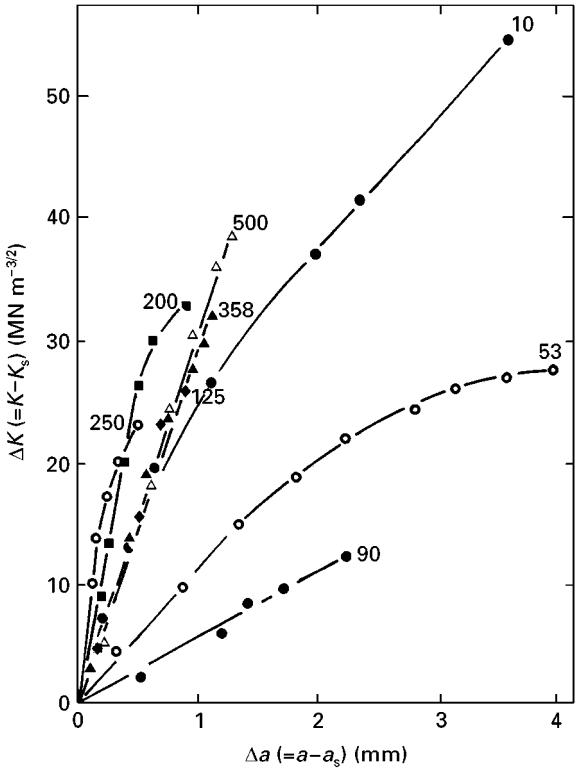

Figure 5 Relationships between ΔK and Δa for specimens containing different amounts of hydrogen (p.p.m.).

fast fracture region is generally the same for specimens with different hydrogen contents and is mainly ductile (Fig. 6). On the other hand, the fractography in the slow cracking region of as-received Ti6Al4V consists of a mixture of dimples and cleavage (Fig. 7a) and with increasing hydrogen the fracture mode remains transgranular until the hydrogen content reaches about 250 p.p.m., although the fractions of cleavage and the dimple size vary, i.e. below 90 p.p.m. the fraction of cleavage is reduced as the hydrogen content increases (Fig. 7). The specimen containing 500 p.p.m. hydrogen shows slightly different fractography, generally with more and finer dimples present as well as secondary cracking (Fig. 7).

The slow crack propagation path as revealed by back-scatter electron imaging is mainly transgranular through the α grains in the as-received material, and mainly intergranular along the interface between α and β phases in the specimen containing 500 p.p.m. hydrogen (Fig. 8 a, b).

TABLE I Macro-characteristics of the fracture surfaces of CT specimens broken after hydriding to different levels

[H] (p.p.m.)	Illustration of fracture surface[a]	Features	The maximum width of the shear lip, W (mm)
10	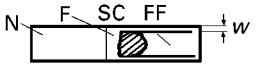	The slow crack growth at the centre	0.21
30		As above	0.125
53		Slow crack also present at the surface	0.12
90		As above	0.115
125	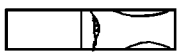	Slow crack growth is very short at the centre	0.96
200	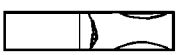	As above	0.95
250	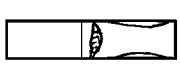	Slow cracking at both surface and centre	0.50
355		As above	0.49
500	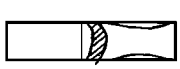	As above	0.185

[a] There are four areas: notch (N); fatigue (F); slow cracking (SC); fast fracture (FF).

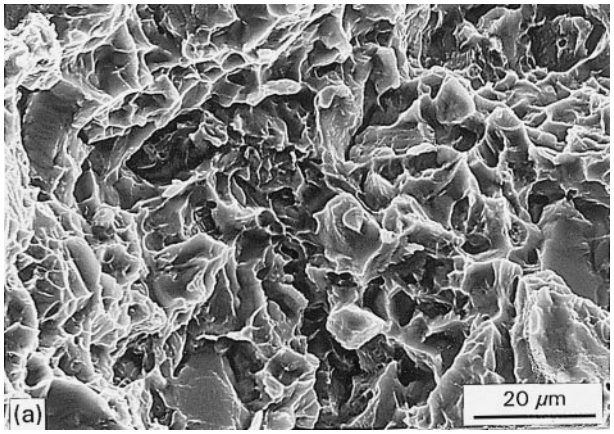

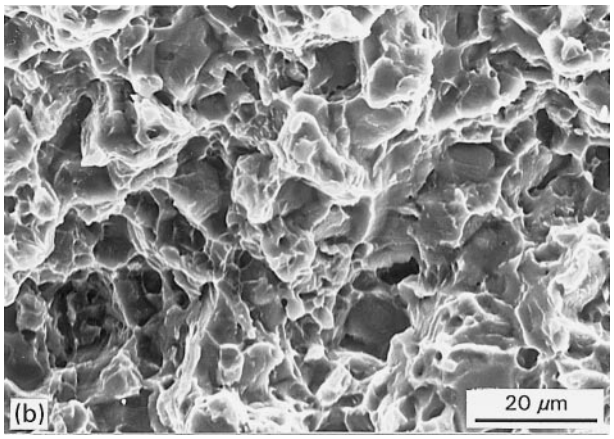

Figure 6 Fractography of the fast fracture region: (a) CT specimen with 10 p.p.m. hydrogen and (b) CT specimen with 500 p.p.m. hydrogen.

4. Discussion

The principal failure processes involved under monotonic load in titanium are creep and environmentally sensitive fracture, and various mechanisms have been proposed [27] to explain the fracture process characteristics. From the point of view of extended service life, the threshold stress intensity factor, K_s, is of greatest importance because components may be expected to operate safely only when the applied stress intensity factor is below the threshold value. Once slow cracking initiates, the dynamics of the crack growth, including the actual growth rate, must be considered for life prediction. Attention must also be paid to the assessment of residual strength by developing crack growth resistance curves (R-curves) that reveal the relationship between crack growth and the applied stress intensity factor [28, 29]. The resistance to crack extension may be expressed in terms of the R-curve slope [30] and the steeper the slope the greater is the crack growth resistance. The relationship between ΔK and Δa was employed in the present work (Fig. 5) in order to facilitate comparison of resistance to crack growth. The ultimate limit for survival is, of course, represented by the critical stress intensity factor, K_H, for fast cracking.

There are obviously two different effects involved with increasing hydrogen content in these results. K_s increases and K_H decreases with hydrogen content up to 90 p.p.m. $\Delta a/\Delta t$ increases drastically, the slopes of ΔK–Δa curves (the resistance to crack growth) decrease, the width of the shear lips decreases, the fraction of cleavage cracking decreases and the dimples

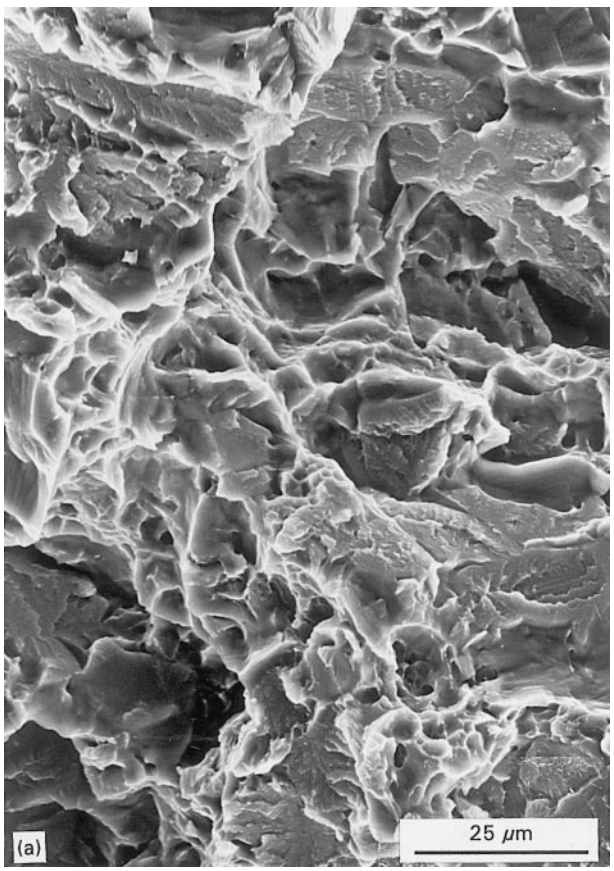

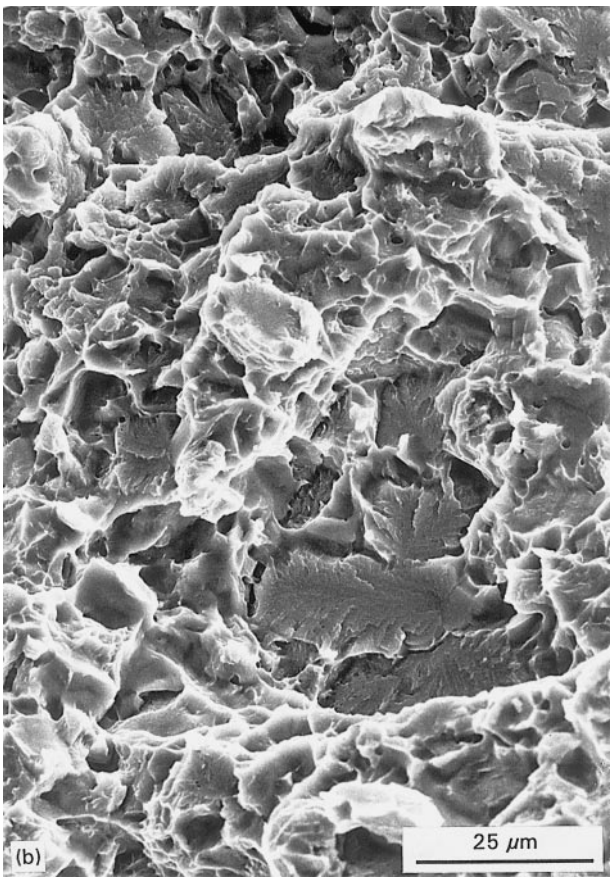

Figure 7 Fractography of the region of slow crack propagation: (a) as-received, (b) 30 p.p.m, (c) 53 p.p.m., (d) 90 p.p.m. and (e) 500 p.p.m. hydrogen.

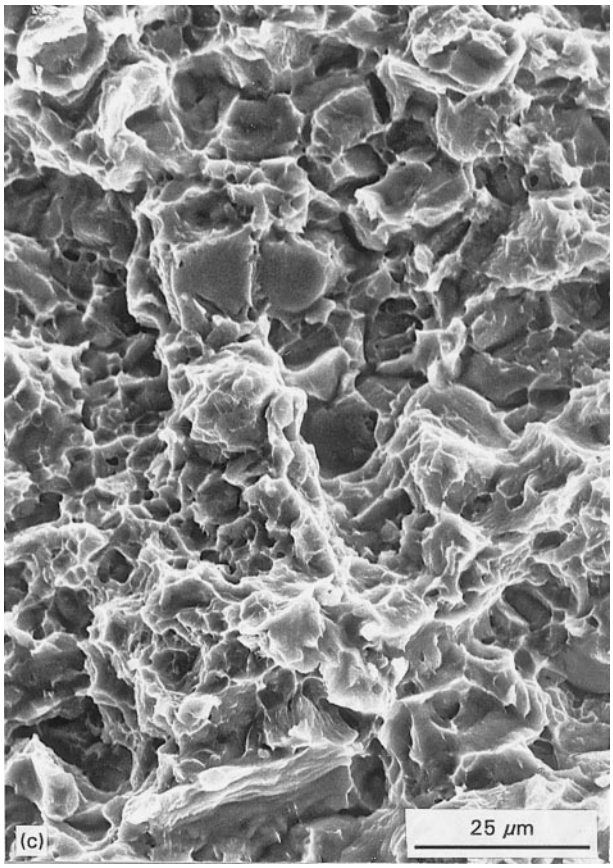

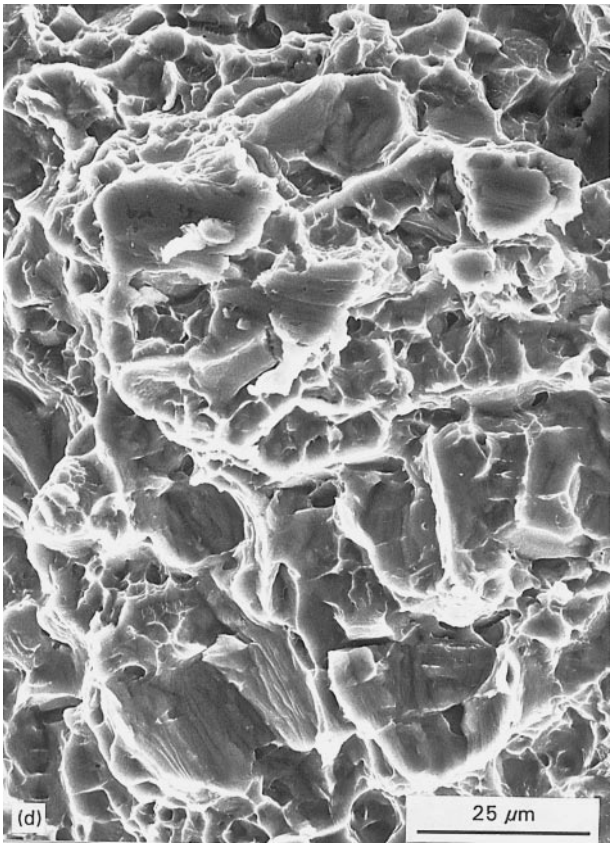

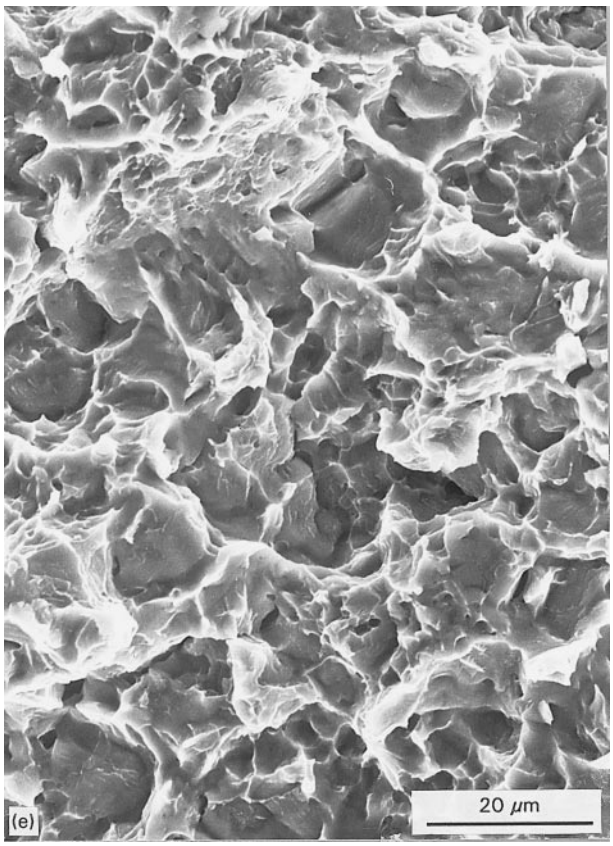

Figure 7 Continued.

become finer and shallower. In contrast, above 125 p.p.m., K_s decreases, $\Delta a/\Delta t$ increases slightly, the ΔK–Δa slope is greater than below 90 p.p.m. but changes very little, the shear lip decreases, and the fractography changes gradually from the mixture of dimples and cleavage to the interfacial separation. The increase in K_s with hydrogen content below 90 p.p.m. suggests that there is greater resistance to crack initiation but, once initiated, cracks propagate rapidly and there seems little resistance to slow crack growth. The principal features of the cracking behaviour at hydrogen concentrations above 125 p.p.m., however, are a decrease in the stress intensity requirements for initiation but little variation in the high resistance to slow crack propagation compared with that at low hydrogen levels. From both points of view, initiation and propagation, there is a deterioration in fracture resistance above about 350 p.p.m., compared with the as-received material.

The tensile test results for smooth specimens with different hydrogen contents in the identical Ti6Al4V bar of the same orientation show that a deterioration in tensile ductility occurs above about 2000 p.p.m. [31], much more than the 350 p.p.m. observed here. The reason for this difference must be that the triaxial stresses at the loaded crack tip can induce enrichment of hydrogen [32, 33], and it is deduced that the enrichment factor involved could be as high as 6. In discussing delayed fracture mechanisms in the α and β titanium alloys containing hydrogen, Daniels *et al.* [34] pointed out in 1959 that some of these failures are the result of creep deformation and some are due to hydrogen-induced cracking, and may be identified by the different electrical resistance changes associated with these two processes. The effect of hydrogen on the creep behaviour has been investigated [3, 16, 34–36] and it was found that hydrogen could induce an increase in creep strain due to its effect in increasing dislocation mobility [35, 36]. Paton and Thompson [37] also discovered that the increase in creep strain

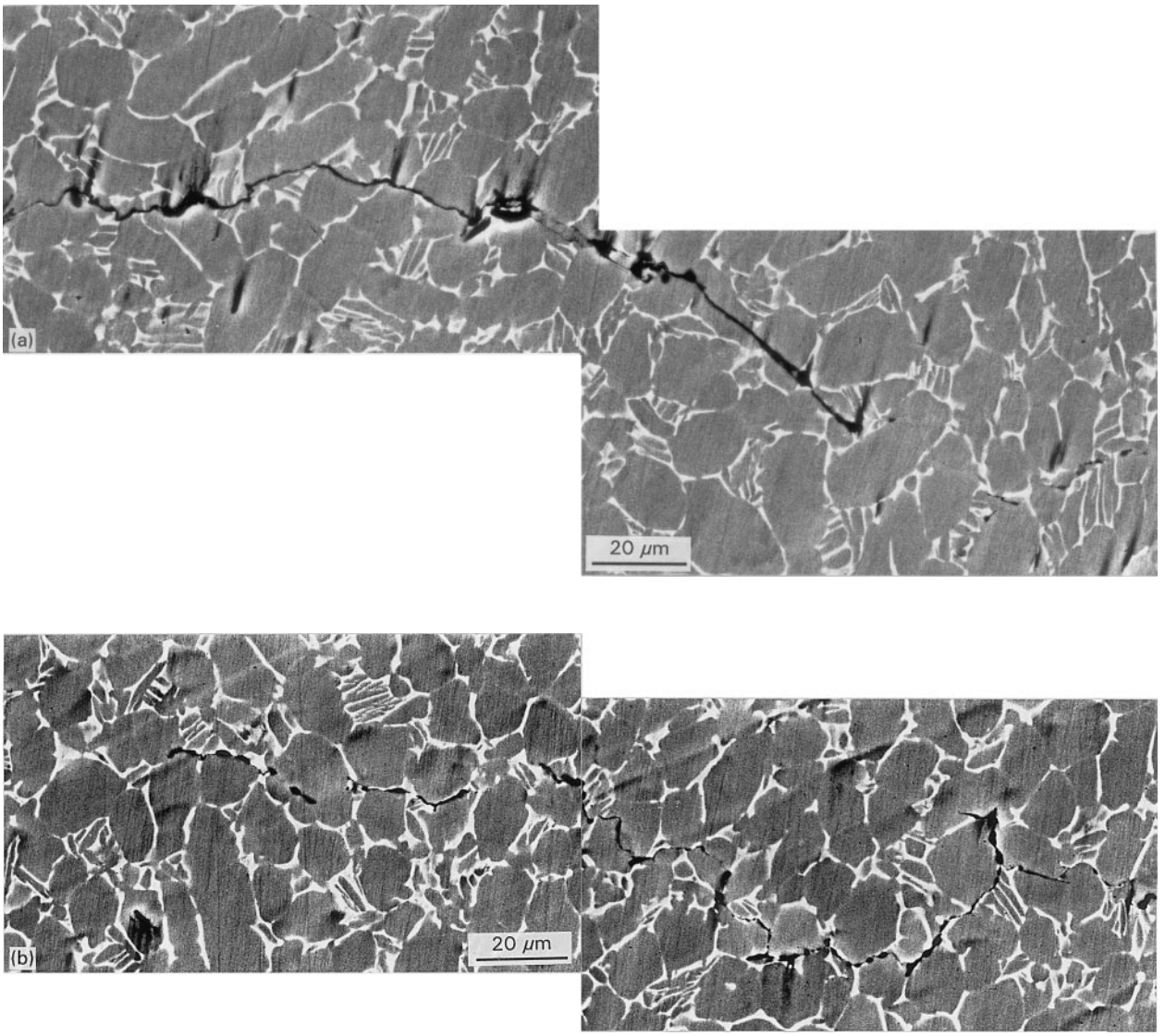

Figure 8 Slow crack propagation path with back-scattered electron imaging: (a) as-received and (b) with 500 p.p.m. hydrogen.

was related to the hydrogen content and, when the hydrogen content was between 12 and 110 p.p.m., no increase in creep strain occurred, but above 180 p.p.m. hydrogen, there was an increase. Williams [3] investigated the effect of hydrogen on sub-critical crack growth in titanium alloys under sustained load, and the experimental results showed that hydrogen in Ti6Al4V produced an increase in K_s and da/dt but a decrease in K_H with hydrogen level from 7 p.p.m to 60 p.p.m., and this resembles the results obtained here below 90 p.p.m. hydrogen. He believed that the abnormal increase in K_s with increasing hydrogen could only be explained in terms of the effect of hydrogen on creep. He also found that hydrogen significantly decreases the rate in secondary creep, then postulated that hydrogen embrittlement requires a finite amount of plastic deformation at the crack root, and the increased creep resistance offsets the increased susceptibility to embrittlement at higher hydrogen content. Sastry *et al.* [16] studied sub-critical crack growth under sustained load in Ti6Al6V2Sn and suggested that the incidence of significant ductile tearing and dimpled fracture in Ti6Al6V2Sn specimens containing low interstitial hydrogen indicates that creep deformation makes a significant contribution to sub-critical crack growth under sustained load.

In the present work, K_s increases with increasing hydrogen below 90 p.p.m., which is not consistent with any reported mechanism of hydrogen embrittlement. In addition, data for the effect of hydrogen on the mechanical behaviour of Ti6Al4V [31] indicate that below 90 p.p.m. the hydrogen atoms occupy the octahedral interstitial sites of the h c p α phase, which does not induce lattice expansion, i.e. the hydrogen partial molar volume is zero and hence the possibility of interaction between the hydrogen and triaxial stresses or dislocations is very small, with the result that enrichment of hydrogen by stress-induced diffusion is highly unlikely.

For further analysis of the current data, the parameter tan α_s may be used to represent the degree of plastic deformation at the crack tip for slow crack initiation. This parameter is defined as:

TABLE II Effect of hydrogen on the incubation period and plastic deformation (fatigue crack opening) involved in initiation of slow crack growth from a fatigue crack of length a_0

	[H] (p.p.m.)									
	10	30	53	90	125	165	200	250	358	500
a_s (mm)	6.79	6.93	6.88	6.92	6.69	7.04	6.69	7.21	7.50	8.28
t_s (min)	690	820	925	1260	1012	1070	1055	1080	642	740
tan α_s	0.070	0.082	0.093	0.126	0.104	0.105	0.109	0.103	0.057	0.062

$\tan \alpha_s = t_s \dot{\varepsilon}/2a_0$ where t_s is the initiation time (incubation period) for the slow crack, $\dot{\varepsilon}$ is the slow strain rate and a_0 is the initial crack length, i.e. from the loading line to the fatigue crack tip. Using this approach, it can be seen (Table II) that with increasing hydrogen content below 90 p.p.m. both t_s and tan α_s increase and also, in connection with the decrease in the cleavage fraction in the fracture surfaces, it might be expected that the lower dissolved hydrogen inhibits cleavage cracking and improves the material ductility, which is consistent with the results of smooth tensile tests [31]. However, as the slow crack grows the crack growth resistance decreases, which mirrors the relationship between creep rate and load; the greater the load the quicker is the creep fracture process. Then, when the hydrogen content exceeds 125 p.p.m., the hydrogen induces an expansion of the α lattice [31] and, as a result, there will be hydrogen enrichment at the loaded crack tip due to interaction between hydrogen and triaxial stress or dislocations. If the degree of enrichment exceeds the hydrogen solubility in the α phase (about 250 p.p.m. [31]), some of the hydrogen would be in the β phase or at the α/β interface. The slow crack growth would then be related to hydrogen enrichment and hydrogen diffusion would control the process determining the crack growth resistance. At room temperature, the diffusivities of hydrogen in the α and β phases are $D_\alpha = 3 \times 10^{-15}\ m^2\ s^{-1}$ and $D_\beta = 2 \times 10^{-12}\ m^2\ s^{-1}$, respectively, and the average slow crack growth rate is 10^{-5}–$10^{-4}\ mm\ s^{-1}$. If the diffusion distance is estimated by $(Dt)^{1/2}$, then the distances diffused in the α and β phases in 1 s are $V_\alpha = 5 \times 10^{-5}\ mm\ s^{-1}$ and $V_\beta = 1.4 \times 10^{-3}\ mm\ s^{-1}$, respectively. Comparison of these data suggests that the diffusion of hydrogen in the α phase is dominant for slow crack growth at lower hydrogen contents, but diffusion in both the α and β phases is involved at higher hydrogen contents. In addition, the hydrogen content will affect the threshold stress intensity factor (Fig. 3), the incubation period (Table II) and the slow crack growth rate (Fig. 4). The higher the hydrogen content, the less is the required stress gradient and incubation period for slow cracking and the faster is the slow crack growth rate. The enrichment of hydrogen occurs mainly in the β phase and at the interface between α and β phases, and brittle hydrides may then form at the latter to become initiation sites for slow cracking. Such initiation at the α/β interface was observed in a specimen containing 500 p.p.m. hydrogen (Fig. 8b).

Whatever the hydrogen content of these particular specimens, fast fracture is invariably preceded by slow crack growth, i.e. K_H is always higher than K_s, despite the occurrence of two different regimes of slow crack growth – above and below 90 p.p.m. hydrogen. There is inevitably a decrease in the stress intensity factor required to produce fast fracture as the amount of hydrogen increases, but between 90 and 250 p.p.m. there is a temporary increase in the apparent value of K_H. The latter is probably caused by the occurrence of crack blunting during the lengthy propagation of the slow crack, as indicated by the high values of tan α_s (Table II).

5. Conclusions

1. The effect of hydrogen on the fracture properties may be divided into two categories according to the hydrogen content. When the concentration is below 90 p.p.m. the hydrogen dissolved as an intersitial atom plays a major role and results in the enhancement of the threshold stress intensity factor but a decrease in the crack propagation resistance and an increasing rate of slow crack growth. The mechanism of slow crack growth is then by creep. When the hydrogen content is above 125 p.p.m., the enrichment of hydrogen at the stressed crack tip due to interaction with the triaxial stress and dislocations reduces the threshold stress intensity factor. The crack growth rate is then controlled by hydrogen diffusion in the α and β phases.

2. In comparison with the fracture properties of as-received material, the deterioration of fracture properties in the hydrogenated materials becomes significant above about 350 p.p.m. hydrogen.

3. The fracture mode in the as-received material is a mixture of dimples and cleavage, but at higher hydrogen levels the initiation and propagation is predominantly along the interfaces between the α and β phases.

4. Final fast fracture is invariably preceded by slow crack growth and $K_H > K_s$, although the fracture surface exhibits the characteristics of ductile failure.

Acknowledgement

This work was carried out whilst Dr Gu was a Senior Visiting Fellow at the Department of Mechanical, Materials and Manufacturing Engineering, The University, Newcastle-upon-Tyne.

References

1. J. D. DESTFANI, "ASM International Metals Handbooks", 10th Edn, Vol. 2 (American Society for Metals, Metals Park, Ohio, USA. 1990) p.586.

2. D. A. MEYN, *Metall. Trans.* **5** (1974) 2405.
3. D. N. WILLIAMS, *Mater. Sci. Eng.* **24** (1976) 53.
4. H. HOEG, B. HOLLUND and I. W. HALL, *Metal Sci.* **14** (1980) 50.
5. A. VASSEL, *J. Less-Common Metals* **69** (1980) 293.
6. X. J. WAN and G. Y. GAO, in "Proceedings of the 5th National Congress on Titanium Alloys", China (1984) p.67.
7. G. F. PITTINATO and S. F. FREDERICK. *Metall. Trans.* **1** (1970) 3241.
8. G. F. PITTINATO, *ibid.* **3** (1972) 235.
9. H. G. NELSON, D. P. WILLIAMS and J. E. STEIN, *ibid.* **3** (1972) 469.
10. D. P. WILLIAMS and H. G. NELSON, *ibid.* **3** (1972) 2107.
11. D. A. MEYN, *ibid.* **3** (1972) 2302.
12. G. H. KOCH, A. J. BURSLE, R. LIU and N. PUGH, *ibid.* **12A** (1981) 1833.
13. H. G. NELSON, *ibid.* **4** (1973) 364.
14. R. R. BOYER and W. F. SPURR, *ibid.* **9A** (1978) 23.
15. N. R.MOODY and W. W. GERBERICH, *ibid.* **11A** (1980) 973.
16. S. M. L. SASTRY, R. J. LEDERICH and B. B. RATH, *ibid.* **12A** (1981) 83.
17. N. R. MOODY and W. W. GERBERICH, *ibid.* **13A** (1982) 1055.
18. H. G. NELSON, *ibid.* **7A** (1976) 621.
19. R. N. PARKINS, in "Stress Corrosion Cracking – The Slow Strain Rate Technique", edited by G. M. Ugianskly and J. H. Payer, ASTM STP 665 (American Society for Testing and Materials, Philadelphia, PA, 1979) p.5.
20. R. N. PARKINS, *Corrrosion* **43** (1987) 130.
21. J. CONGLETON and R. N. PARKINS, *ibid.* **44** (1988) 290.
22. D. HARDIE and D. DONG, *Br. Corros. J.* **29** (1994) 156.
23. J. GU and D. HARDIE, *J. Mater. Sci.* **31** (1996)
24. British Standard, BS5447 (1977) "Methods of test for plane strain fracture toughness (K_{I_c}) of metallic materials".
25. P. ALBRECHT, *J. Test. Eval.* **10** (1982) 245.
26. S. M. L. SASTRY, P. S. PAO and K. K. SANKARAN, in "Proc 4th International Conference on Titanium Science and Technology" edited by H. Kimura and O. Izumi, Vol. 3 (1980) p.873.
27. A. S. TETELMEN and A. J. McEVILY, "Fracture of Structural Materials" (Wiley, New York, 1967) p.403.
28. R. H. HEYER, "Fracture Toughness Evaluation by R-Curve Methods", ASTM STP 527 (American Society for Testing and Materials, Philadelphia, PA, 1973) p.3.
29. D. Y. WANG, "Mechanics of Crack Growth", ASTM STP 590 (American Society for Testing and Materials, Philadelphia, PA, 1976) p.169.
30. R. W. JUDY and R. J. GOODE, "Fracture Toughness Evaluation by the R-Curve Method", ASTM STP 527 (American Society for Testing and Materials, Philadelphia, PA, 1973) p.48.
31. D. HARDIE and J. GU, *Mater. Sci. Technol.*, in press.
32. A. R. TROIANO, *Trans. ASM* **52** (1960) 54.
33. G. M. PRESSOUYRE, *Metall. Trans.* **10A** (1979) 1571.
34. R. D. DANIELS, R. J. QUIGG and A. R. TROIANO, *Trans. ASM* **51** (1959) 843.
35. D. S.SHIN, I. M. ROBERTSON and H. K. BIRNBAUM, *Acta Metall.* **36** (1988) 111.
36. G. T. GAO and S. C. DEXTER, *Metall. Trans.* **18A** (1987) 1125.
37. N. E. PATON and A. W. THOMPSON, *ibid.* **13A** (1982) 1531.

Received 16 February
and accepted 18 *March* 1996